Supporting Information for "Column-Compound Extremes in the Global Ocean"

Contents of this file

1. Text S1 to S4

(i) Text S1 - Detrending the data for the fixed and moving baselines.

(ii) Text S2 - Sensitivity cases of minimum vertical threshold of CCXs.

(iii) Text S3 - K-means clustering of CCX types into regions.

2. Figures S1 to SX

(i) Figure S1 - Mean absolute percentage error of the quadratic trend of $[H^+]$ at depths of 5m, 145m, and 285m.

(ii) Figure S2 - Top: Mean absolute percentage error of the quadratic trend of $[H^+]$, at $5\,m$ for the month of January. Bottom: Annual time series of $[H^+]$ and the fitted quadratic trend at selected points within the map.

(iii) Figure S3-S6 - Sensitivity cases of different column thresholds using mean CCX days per year.

(iv) Figure S7 - Evaluation of CESM $20\,°C$ isotherm depth, against ORAS5 reanalysis.

(v) Figure S8 - Key metrics of MHW-LOX events in the global ocean.

Corresponding author: J. Wong, CHN E29, Universitätstrasse 16, 8092 Zürich, Switzerland (joel.wong@usys.ethz.ch)

September 27, 2023, 10:45pm

19   (vi) Figure S9 - Key metrics of OAX-LOX events in the global ocean.

20   (vii) Figure S10 - Plots supporting choice of cluster number for k-means clustering.

21   (viii) Figure S11 - Annual time series of CCX volume fraction divided by clusters.

22 **Additional Supporting Information (Files uploaded separately)**

23   1. Captions for Movie S1

24   (i) Video of vertical section detected single extremes of the equatorial Pacific during

25 1998, at a daily resolution.

Text S1 - Detrending the data for the fixed and moving baselines.

The temperature, $[H^+]$, and $[O_2]$ values from the hindcast were detrended to remove the trend due to climate change over time. Due to the steep increase in $[H^+]$ over the hindcast period, a quadratic trend was chosen to represent this increase (Hauri et al., 2021). For the sake of consistency, a quadratic trend was also used to detrend temperature and $[O_2]$ values, even though their rate of increase is closer to a linear trend. In Figures S1 to **??**, we plot the mean absolute percentage error (MAPE) of the fitted quadratic trend in each month, and three depth levels. The maximum MAPE across all grid cells and depths is 28%. In areas with the highest MAPE, we found that the error was a result of high interannual variability of $[H^+]$ values. We show this in Figure S2, where the quadratic function fits the overarching trend, but the high variability leads to relatively higher error.

The procedure used to detrend the data is as follows. Temperature, $[H^+]$, and $[O_2]$ values from the hindcast were first monthly-averaged in each grid cell. A quadratic trend is then fitted on the variables in each month and grid cell, over 63 (1958-2020) years of the hindcast. The values of the variables were then detrended to the year 1958, using the monthly fitting coefficients of the quadratic trend. Finally, the seasonal threshold with baseline of 1958 was obtained by taking the 95th (5th) percentile of temperature, $[H^+]$, and $[O_2]$ values over an 11-day rolling window. That is, a total of (63 years $*$ 11 days $=$ 693) values are used to determine the threshold for each day of year.

During detection on a fixed baseline, the non-detrended variables are used, against the 1958 baseline calculated earlier. On a moving baseline, the quadratic trend is added to the 1958 baseline threshold for each year, so that the threshold increases (or decreases for O_2) with the year of the hindcast.

Text S2 - Sensitivity cases of minimum vertical threshold of CCXs.

A threshold of at least $50\,m$ out of the $300\,m$ column is chosen as the definition of a column extreme event. This value was chosen such that a significant fraction (at least $16\,\%$) of the column is occupied by extremes under this definition. Using too small a threshold diminishes the biological relevance of the definition. On the other hand, too large a threshold limits the number of detected extreme events in this study. The considerations behind the choice of this threshold is similar to that of percentile thresholds in MHW studies.

Apart of $50\,m$, we conducted a sensitivity test of using $25\,m$, $75\,m$, and $100\,m$ as the column extreme threshold. Under such threshold changes, we expect the number of detected extreme days to decrease (increase) as the threshold increases (decreases). Upon comparing the mean extreme days per year for each case, we found no significant change in the regional distribution of CCXs. In some regions where the threshold is stricter, we no longer detect CCXs when compared to the $50\,m$ case. Some examples of this include central tropical Pacific, and tropical Indian ocean. These comparison plots are presented in Figures S3-S6 of the supporting information.

Text S3 - K-means clustering of CCX types into regions.

The detected CCXs were regionally clustered using k-means clustering as part of the analysis of their drivers. The dimensions used in the clustering are the vertical locations of single grid cell extremes that occurred as part of a CCX, weighted by the intensity index. First, 6 bins of $50\,m$ each are defined for each single extreme type. Over the entire period of the hindcast, the intensity index of each grid cell single extreme is added to these bins. Finally, k-means clustering is performed on these binned counts of intensity index. Double CCXs are clustered on 12 dimensions, while the triple CCX is clustered on 18 dimensions.

To determine the appropriate number of clusters to be used for each extreme type, computed the sum of squares error (SSE), and Silhouette coefficient for $2-6$ clusters. These values are shown in Figure S10 of the supporting information. The number of clusters for each CCX type was chosen by the Elbow method (using the SSE), and maximising the Silhouette coefficient. One exception to the Elbow method is in MHW-OAX-LOW extremes, where 5 clusters were chosen over 4, since the SSE decreased while the Silhouette coefficient increased.

Video of vertical section of the equatorial Pacific during years 1997-1999.

References

Hauri, C., Pagès, R., McDonnell, A. M., Stuecker, M. F., Danielson, S. L., Hedstrom, K., . . . Doney, S. C. (2021). Modulation of ocean acidification by decadal climate variability in the Gulf of Alaska. *Communications Earth and Environment*, *2*(1), 1–7. Retrieved from `http://dx.doi.org/10.1038/s43247-021-00254-z` doi: 10.1038/ s43247-021-00254-z

Mean MAPE (%) of quadratic trend
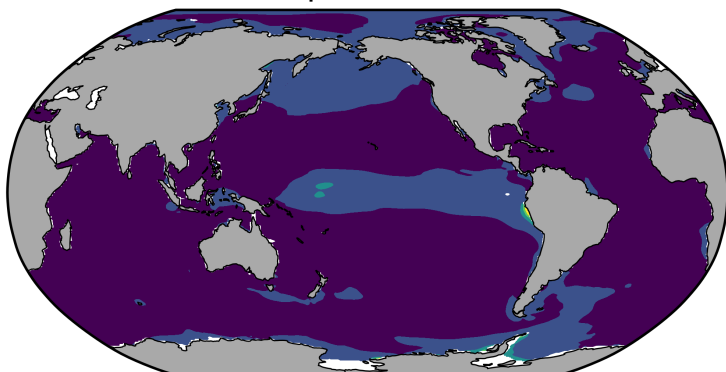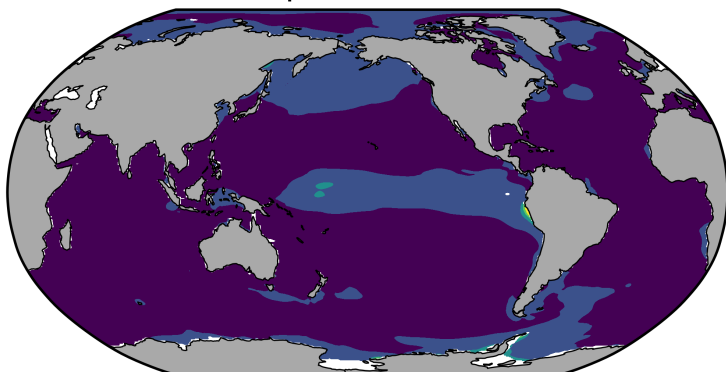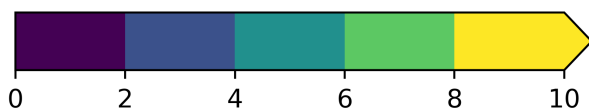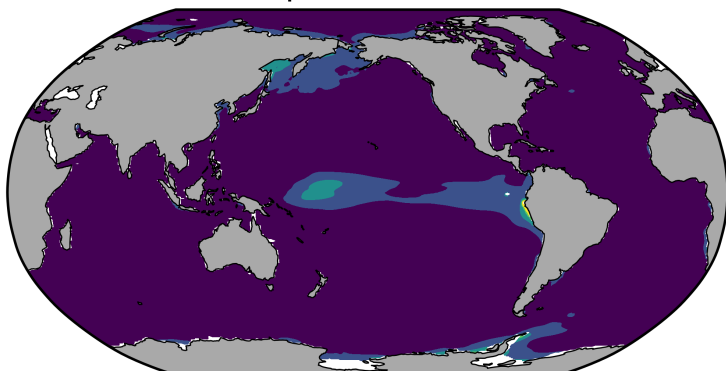
**Figure S1.** Mean absolute percentage error of the quadratic trend of $[H^+]$ at depths of 5m, 145m, and 285m.
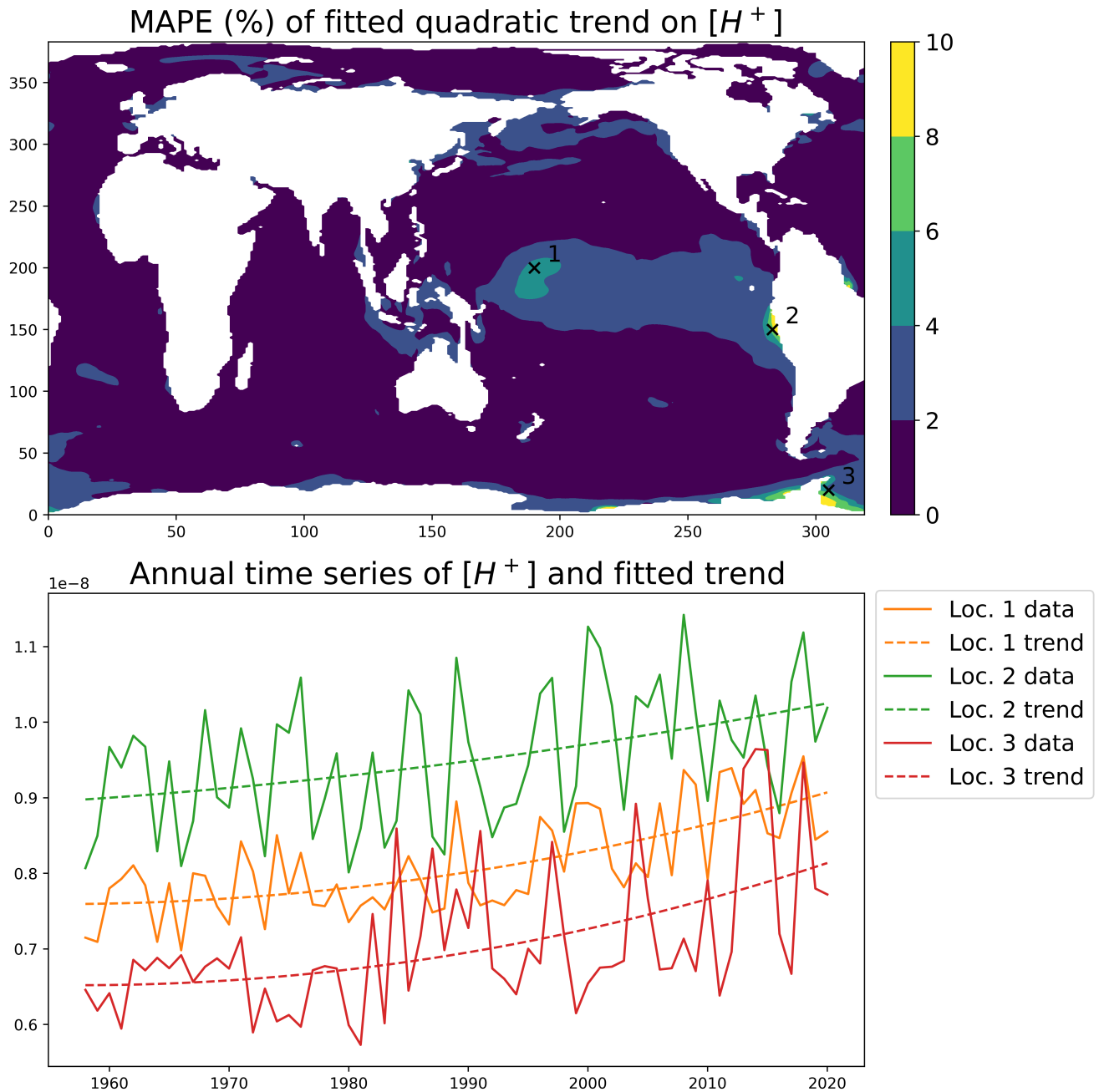
Figure S2. Top: Mean absolute percentage error of the quadratic trend of $[H^+]$, at $5\,m$ for the month of January. Bottom: Annual time series of $[H^+]$ and the fitted quadratic trend at selected points within the map.
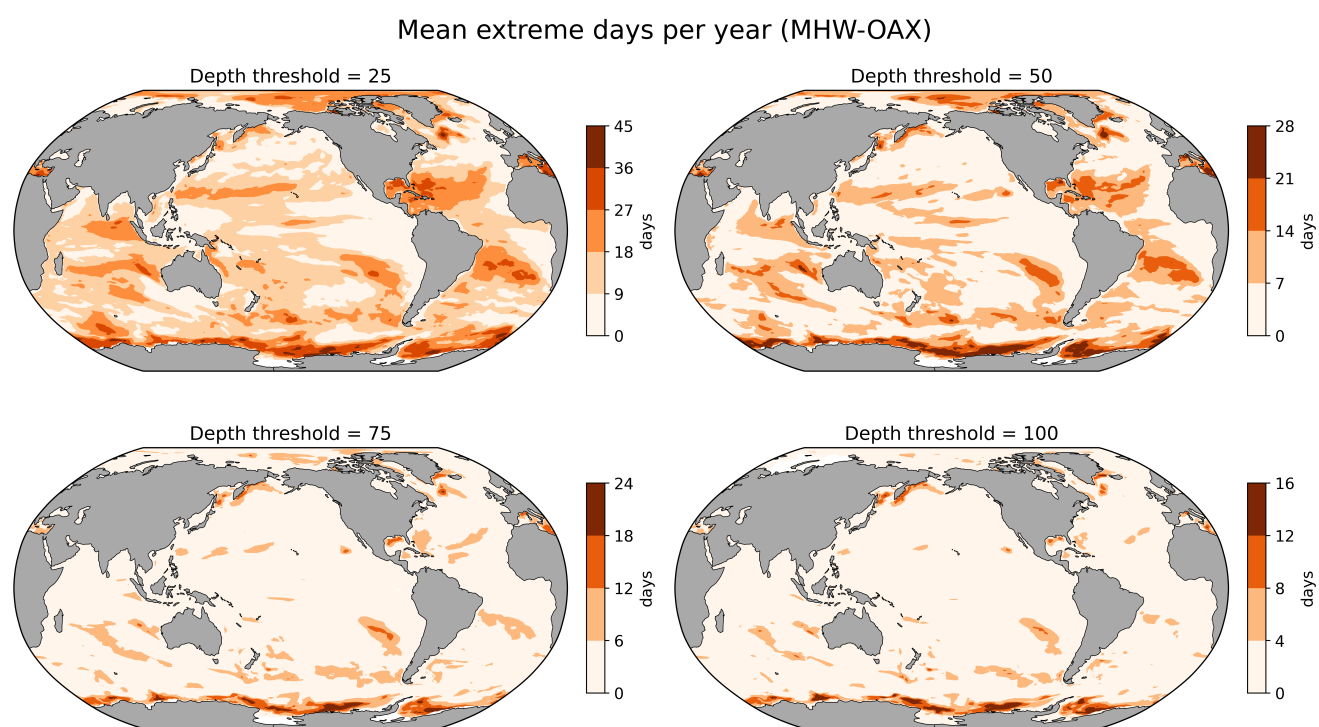
Figure S3.   Sensitivity cases of different column thresholds on the mean CCX days per year of MHW-OAX.

Mean extreme days per year (MHW-LOX)
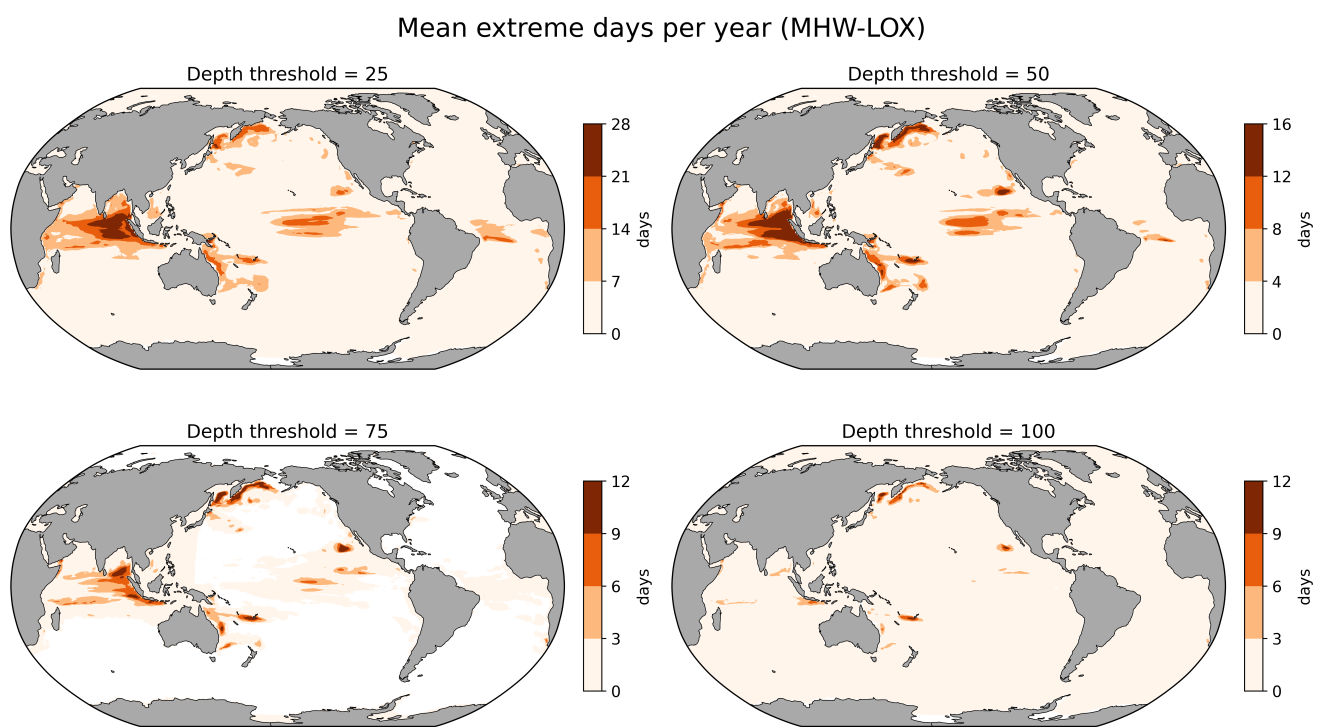
Figure S4.   Sensitivity cases of different column thresholds on the mean CCX days per year of MHW-LOX.

Mean extreme days per year (OAX-LOX)
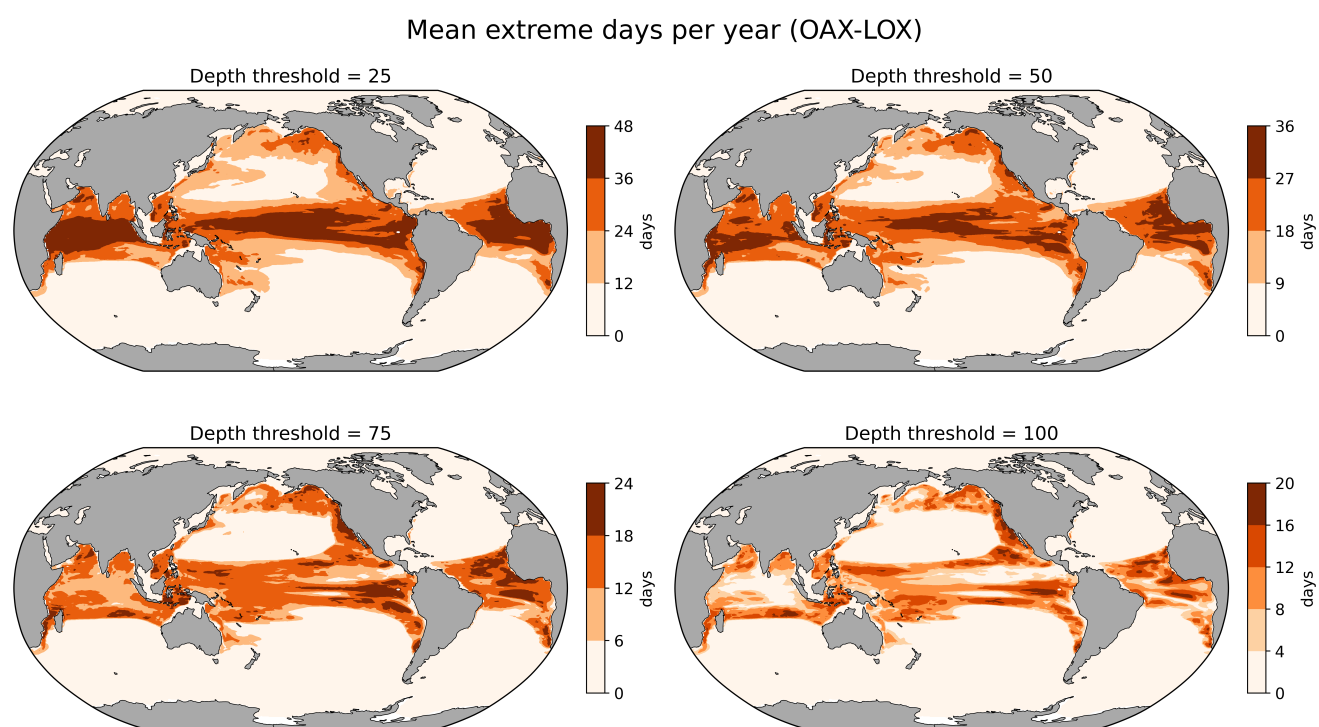
Figure S5.   Sensitivity cases of different column thresholds on the mean CCX days per year of OAX-LOX.

Mean extreme days per year (MHW-OAX-LOX)
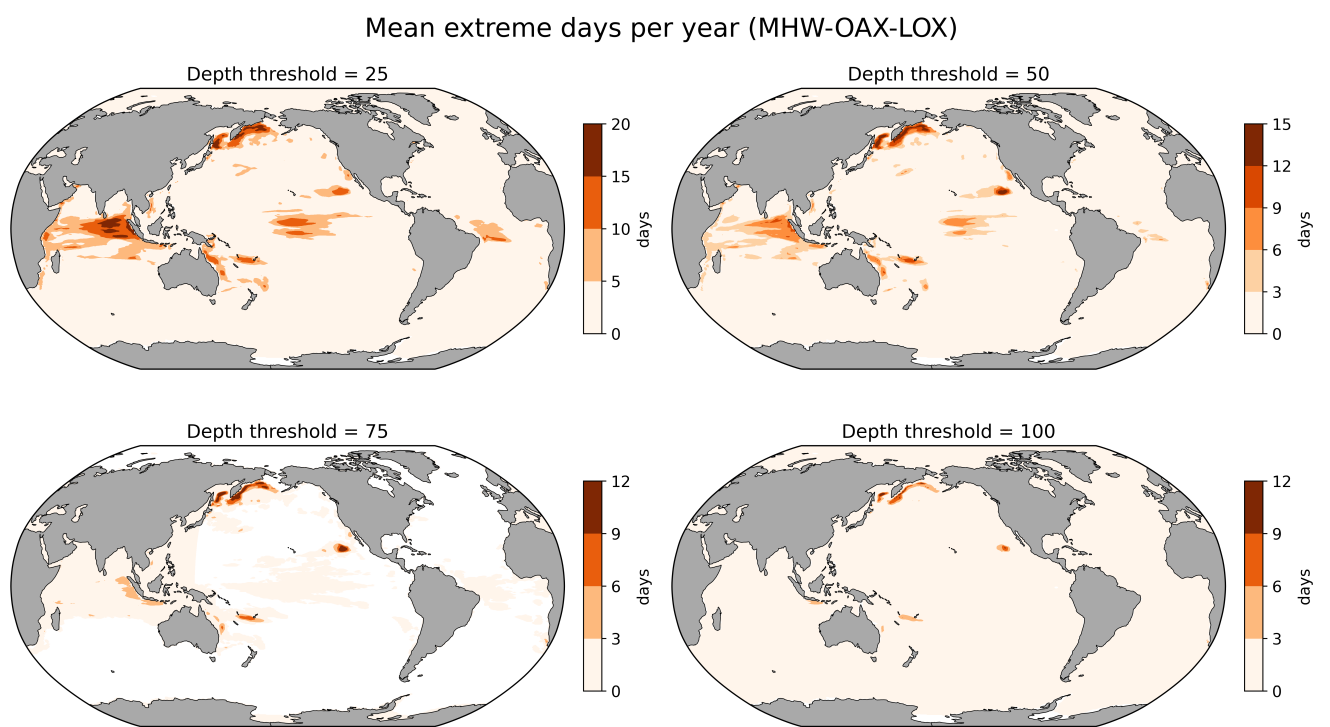
Figure S6.   Sensitivity cases of different column thresholds on the mean CCX days per year of MHW-OAX-LOX.
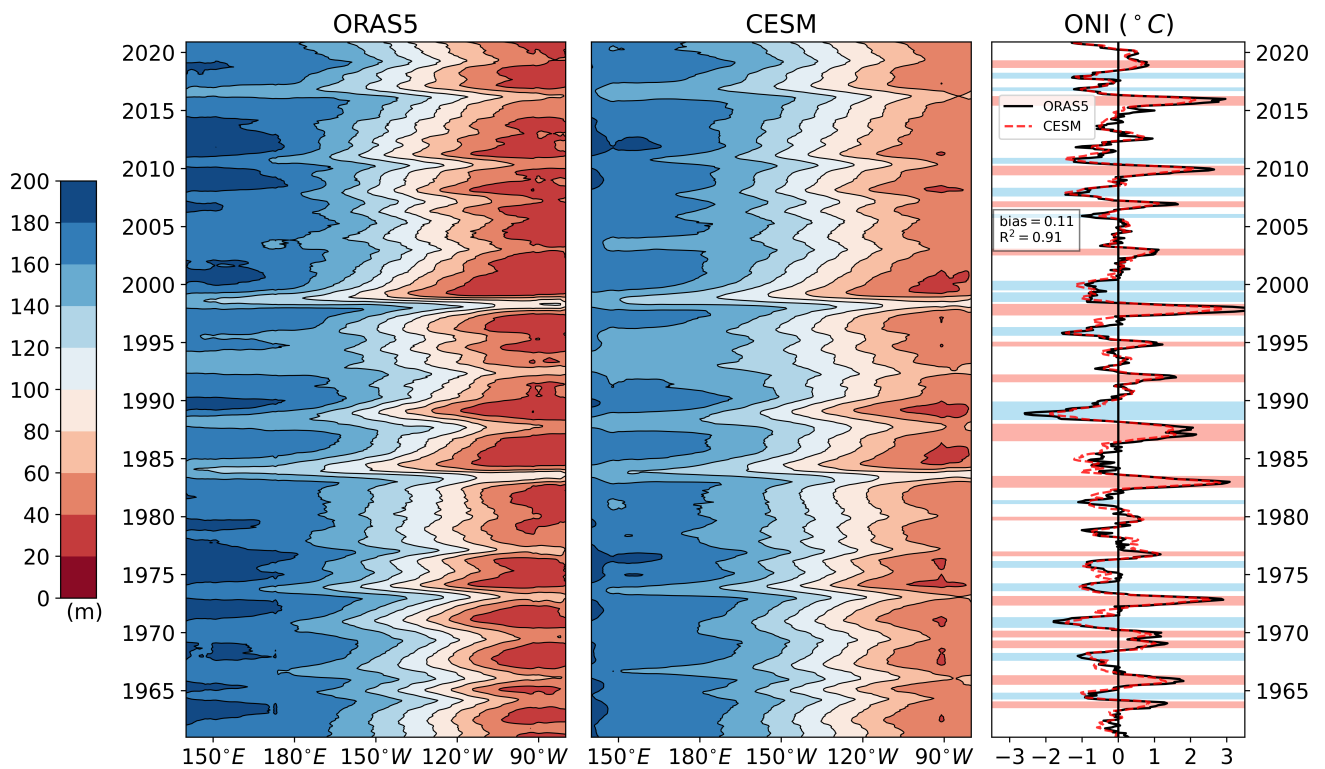
Figure S7.   Evaluation of CESM 20 °C isotherm depth, against ORAS5 re-analysis. A time-series of ONI from CESM (black dotted) and ORAS5 (red solid) is shown on the right, where El Niño periods are shaded in red, and La Niña in blue.
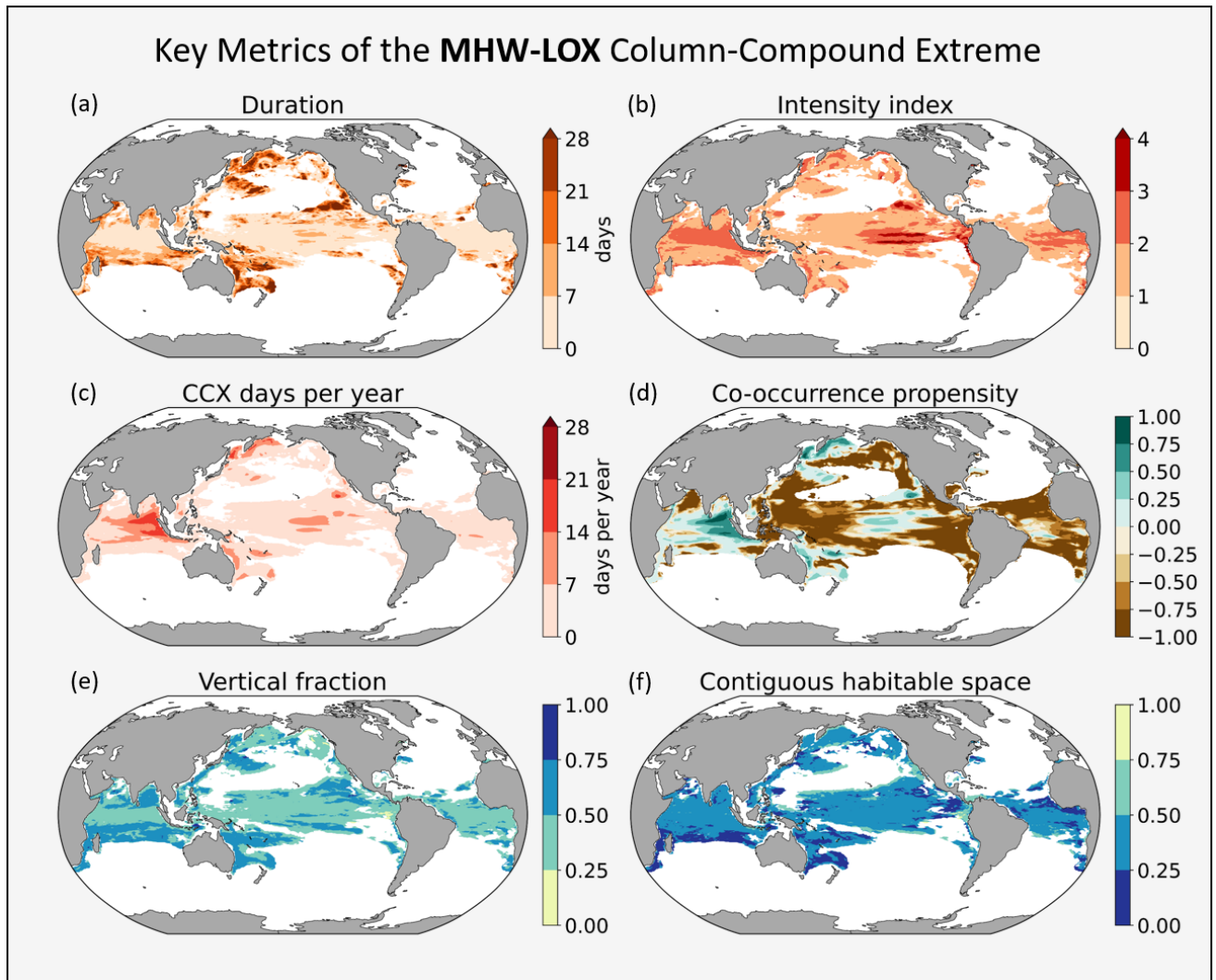
Figure S8. Key metrics of MHW-LOX events in the global ocean. (a) Mean duration, (b) mean annual maximum intensity index, (c) mean days per year, (d) mean co-occurrence propensity, (e) mean fraction of water column occupied by extremes, and (f) mean fraction of contiguous habitable space in the vertical column
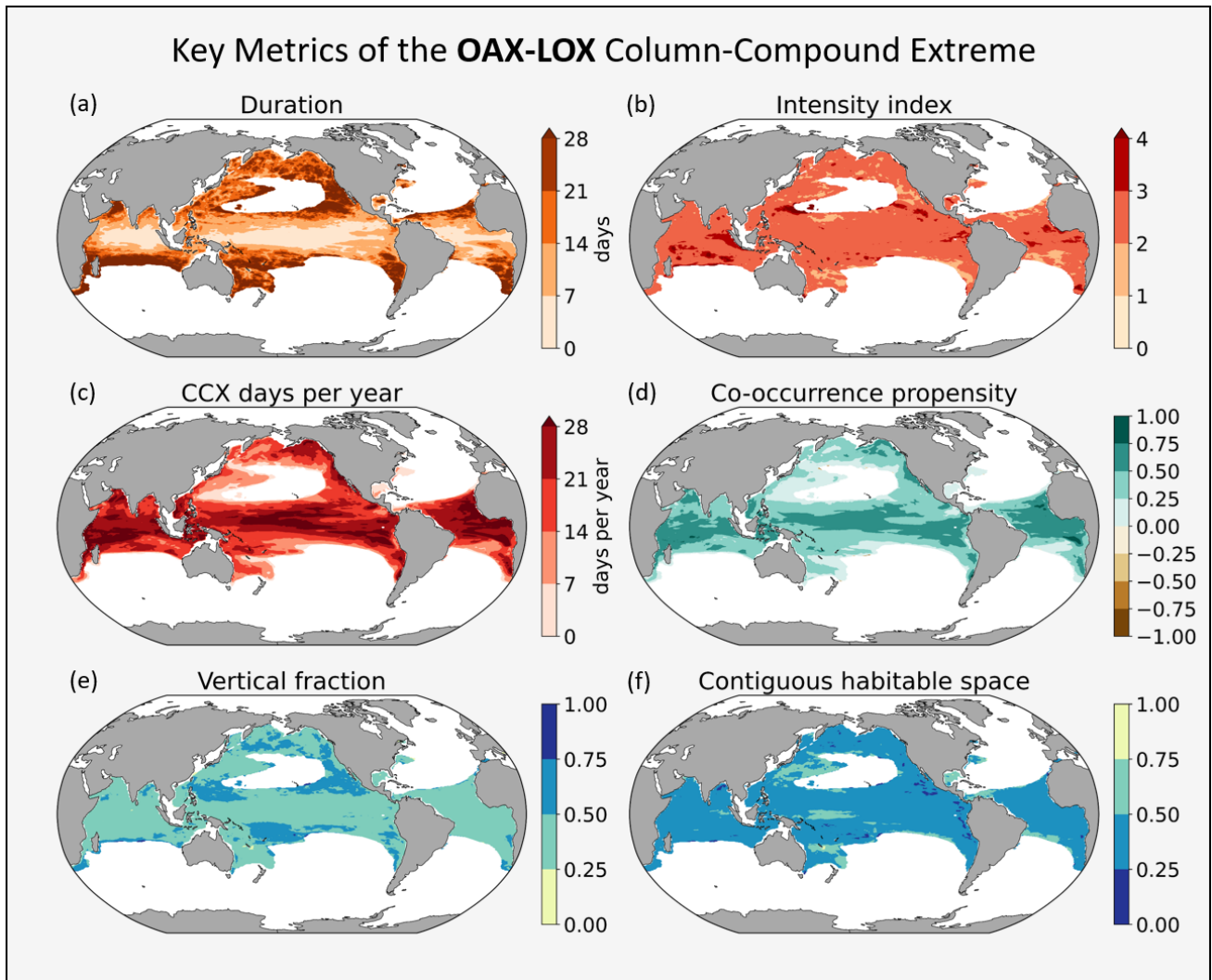
Figure S9.   Key metrics of OAX-LOX events in the global ocean. (a) Mean duration, (b) mean annual maximum intensity index, (c) mean days per year, (d) mean co-occurrence propensity, (e) mean fraction of water column occupied by extremes, and (f) mean fraction of contiguous habitable space in the vertical column
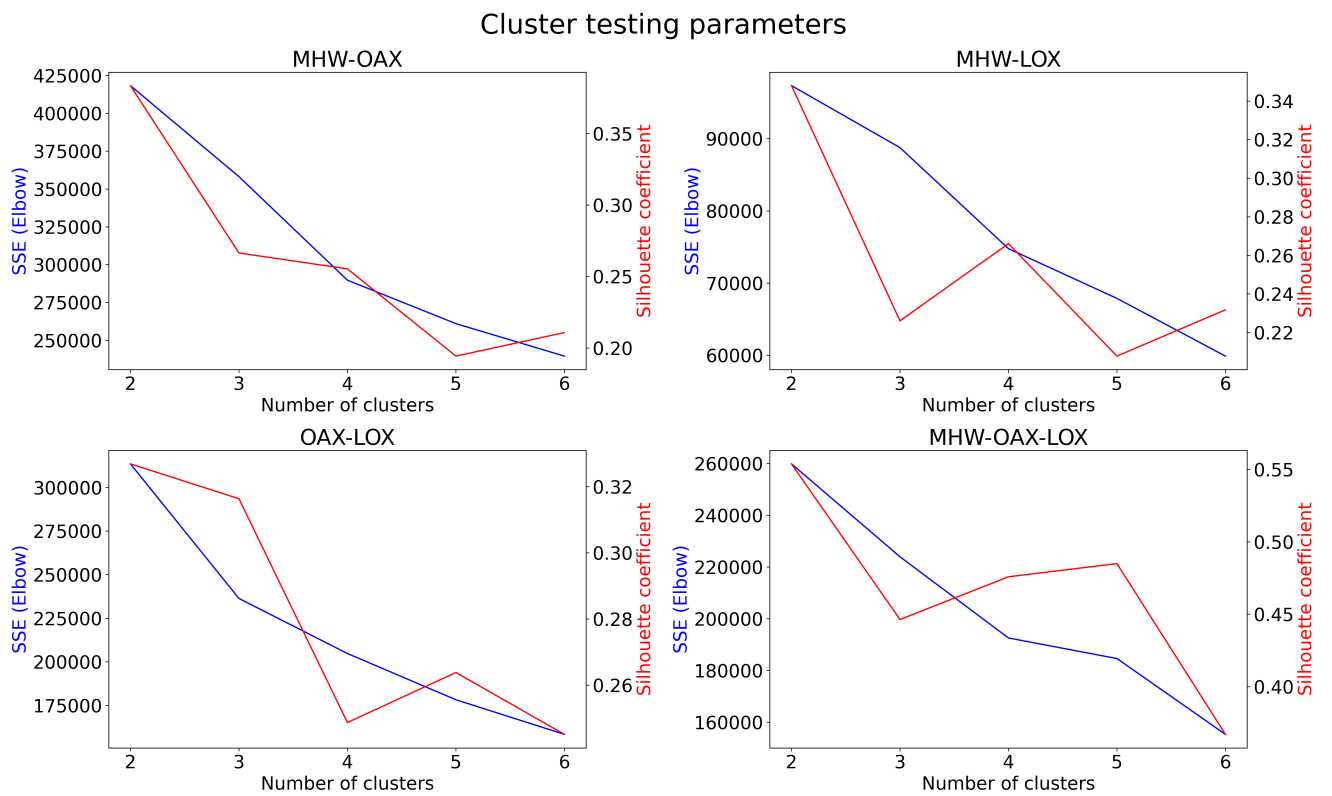
Figure S10.   Sum of square errors (SSE) and Silhouette coefficient for 2-6 clusters for each type of CCX.

Figure S11.   Annual time series of CCX volume fraction divided by clusters.